Mechanistic insights into the regulation of plant phosphate homeostasis by the rice SPX2 – PHR2 complex

Zeyuan Guan
Huazhong Agriculture University https://orcid.org/0000-0002-8909-866X
Qunxia Zhang
Huazhong Agricultural University
Zhifei Zhang
Huazhong Agricultural University
Julie Savarin
University of Geneva
Jiaqi Zuo
Huazhong Agricultural University
Juan Chen
Huazhong Agricultural University
Larissa Broger
University of Geneva
Peng Cheng
Huazhong Agricultural University
Qiang Wang
College of Life Sciences and Technology, Huazhong Aricultural University
Kai Pei
Huazhong Agricultural University
Delin Zhang
Huazhong Agricultural University
Tingting Zou
Huazhong Agricultural University https://orcid.org/0000-0002-7240-1378
Junjie Yan
Huazhong Agricultural University
Ping Yin
National Key Laboratory of Crop Genetic Improvement and National Centre of Plant Gene Research, Huazhong Agricultural University, Wuhan 430070, China https://orcid.org/0000-0001-8001-221X
Michael Hothorn
University of Geneva https://orcid.org/0000-0002-3597-5698

Zhu Liu (liuzhu@mail.hzau.edu.cn)
Huazhong Agricultural University https://orcid.org/0000-0003-4073-7237

Article

Keywords: plant phosphate homeostatis, PHR, PP-InsPs

Posted Date: August 11th, 2021

DOI: https://doi.org/10.21203/rs.3.rs-653544/v1

Version of Record: A version of this preprint was published at Nature Communications on March 24th, 2022. See the published version at https://doi.org/10.1038/s41467-022-29275-8.

Abstract

Phosphate (Pi) is a key macronutrient limiting plant growth and crop productivity. In response to the nutrient deficiency, Pi starvation response (PHR) transcription factors activate Pi starvation induced (PSI) genes. PHR transcription factors are negatively regulated by stand-alone SPX proteins, cellular receptors for inositol pyrophosphate (PP-InsP) nutrient messengers. How PP-InsP-bound SPX domains interact with PHR transcription factors is poorly understood. Here, we report crystal structures of the rice SPX2/$InsP_6$/PHR2 complex and of the PHR2 DNA binding (MYB) domain in complex with its target DNA at resolutions of 3.1 Å and 2.7 Å, respectively. Inositol polyphosphate binding causes SPX2 to assemble into a domain-swapped dimer. The signalling-active SPX2 dimer binds two copies of PHR2, targeting both its coiled-coil (CC) oligomerisation domain and its MYB domain. Structural comparisons, biochemical analyses and genetic characterizations reveal that the SPX2 senses $InsP_6$ / PP-InsPs to inactivate PHR2 by establishing severe steric clashes with the PHR2 MYB domain, preventing DNA binding, and by disrupting oligomerisation of the PHR2 CC domain, attenuating promoter binding. The complex structure rationalizes how PP-InsPs activate SPX receptor proteins to target PHR family transcription factors and provides a mechanistic framework to engineer crops with improved phosphate use efficiency.

Background

Phosphorus is an essential nutrient limiting plant growth, development, and crop productivity[1,2]. Plants have developed sophisticated signal systems to perceive, uptake, transport, and store phosphate (Pi) for the maintenance of Pi homeostasis[3-10]. During Pi limitation, a broad range of Pi starvation induced (PSI) genes are expressed in response to the nutrient deficiency[11-14]. Central regulators responsible for the transcriptional activation of PSI genes are the highly conserved Pi starvation response (PHR) transcription factors[14-18]. Under Pi starvation, rice (*Oryza sativa*) PHR2 (OsPHR2) binds to a *cis*-element (P1BS) in the promoter of various PSI genes and up-regulates their transcription, thus optimizing rice Pi acquisition and utilisation[19-21]. In contrast, under Pi sufficient conditions, an inositol pyrophosphates (PP-InsPs) dependent negative regulator, the stand-alone SPX (SYG1/Pho81/XPR1) protein, binds to OsPHR2 and inactivates its transcriptional activity[19,20,22,23] (Supplementary Fig. 1). Despite extensive studies on the rice PHR signalling pathway, how the SPX protein senses the Pi-level correlated PP-InsPs signal and transduces this signal into transcription repression remains largely unknown.

To reveal this underlying mechanism at molecular level, we sought to determine the structure of rice SPX2 in complex with rice PHR2 and $InsP_6$. We first constructed a PHR2 boundary $PHR2^{225-362}$ containing the MYB domain and the CC domain[16,24,25]. By co-expressing His-tagged $PHR2^{225-362}$ with SPX2 following Ni-NTA pull-down assay, we found that the interaction between $PHR2^{225-362}$ and SPX2 is $InsP_6$ dependent (Supplementary Fig. 2), in agreement with previous reports[22,26]. Initial crystals of the of the SPX2/$InsP_6$/$PHR2^{225-362}$ ternary complex diffracted only to low resolutions. We next identified poorly conserved loop regions in rice SPX2 (residues 36-69 and 191-280; Supplementary Fig. 3). Deletion of

non-conserved insertions represents one promising approach to improve protein stability and crystallizability[27]. Based on this we expressed an engineered SPX$^{21\text{-}202/\Delta 47\text{-}59}$ construct fused to the C-terminus of the macro domain of human histone mH2A1.1$^{181\text{-}366}$ for carrier-driven crystallization[27]. The crystal structure of the mH2A1.1$^{181\text{-}366}$ tagged SPX2$^{1\text{-}202/\Delta 47\text{-}59}$/$InsP_6$/PHR2$^{225\text{-}362}$ ternary complex was subsequently determined at 3.1 Å resolution, using $InsP_6$ (phytic acid) as a commercially available surrogate for the bioactive PP-InsPs[22,25] (Fig. 1a, Supplementary Fig. 4, and Supplementary Table 1). In the complex structure, two $InsP_6$ molecules bind to an SPX2 dimer, and two copies of PHR2 wrap around this dimer. In order to check and assess if the mH2A1.1$^{181\text{-}366}$ fusion tag and the loop truncations may affect the SPX2 structure and its ability to bind PHR2, we performed in solution analytical ultracentrifugation (AUC) and small-angle X-ray scattering (SAXS) analyses of the full-length SPX2$^{1\text{-}280}$/PHR2$^{225\text{-}362}$ complex and a SPX2$^{1\text{-}202}$/PHR2$^{225\text{-}362}$ complex in the presence of 1 mM $InsP_6$, respectively (Supplementary Figs. 5 and 6). We found that the full-length SPX2$^{1\text{-}280}$ binds PHR2$^{225\text{-}362}$ with 2:2 stoichiometry ratio, consistent with the complex crystal structure (Supplementary Fig. 5). In line with this, the SAXS profile derived from the crystal structure is consistent with that observed in solution (Supplementary Fig. 6). Taken together, the AUC and SAXS experiments corroborate the crystal structure of the ternary SPX2$^{1\text{-}202/\Delta 47\text{-}59}$/$InsP_6$/PHR2$^{225\text{-}362}$ complex.

In the SPX2/$InsP_6$/PHR2 complex, the SPX2 dimer obtains a domain-swapped conformation, in which the N-terminal domain of one SPX2 protomer interacts with the C-terminal domain of the other SPX2 protomer, forming an intertwined dimer (Fig. 1b). Specifically, the domain swap involves helices α1 and α2 (NTD) from one protomer and helices α4 and α5 (CTD) from another protomer, which are bridged by two antiparallel extended helices α3 from these two protomers. We validated this dimeric conformation in solution by thiol-directed chemical crosslinking (Supplementary Fig. 7). Rice SPX2 is a stand-alone SPX protein, and a 3-dimensional structural homology search with the program DALI[28] revealed that its dimeric conformation has not been previously observed with other SPX domain structures [22,29] (Figs. 1c, d). SPX domain-containing proteins for which ligand-bound structures are available, such as *Chaetomium Thermophilum* glycerophosphodiester phosphodiesterase 1 (SPX^{CtGde1}) or Vacuolar transporter chaperone 4 (SPX^{CtVtc4}), $InsP_6$ binds the monomeric SPX domain in a 1:1 stoichiometry ratio (Fig. 1c). In these previous structures, core helices α3 and α4 bridge helices α1, α2, α5 and α6, stabilizing a monomeric fold, and $InsP_6$ mainly interacts with helices α2 and α4. In contrast, the rice SPX2 adopts a domain-swapped dimer conformation and coordinates two $InsP_6$ molecules in a 2:2 stoichiometry ratio. The helix α2 of one protomer and the helix α3 of another protomer form the basic binding surface for $InsP_6$ / PP-InsPs.

To assess the recognition of inositol pyrophosphate signal by the domain-swapped rice SPX2 dimer, we performed extensive mutational analyses of the $InsP_6$ / PP-InsP binding site. We co-expressed 8×His-tagged PHR2$^{225\text{-}362}$ and untagged wild-type vs. mutant SPX2$^{1\text{-}280}$ and assessed their interaction in Ni-NTA pull-downs in vitro (see Methods). $InsP_6$ binds to a positively charged surface by a set of highly

conserved residues in SPX proteins[22] (Figs. 2a, b; Supplementary Fig. 3). The binding surface in rice SPX2 is formed by the basic residues K26, K29 and R31 from protomer A, and K143, K146, K147 and K150 from protomer B of the SPX2 dimer. The highly conserved Y25 and L28 also contribute the binding surface. In line with this, the Y25F, Y25A, L28A, K29A, or K143A/K147A mutations strongly reduced/abolished $InsP_6$ binding in vitro (Fig. 2c). Single amino-acid substitutions in the SPX basic binding surface had little effect on $InsP_6$ binding (Fig 2c). The area of the positively charged accessible surface for $InsP_6$ binding is larger than the shape of negatively charged $InsP_6$ (Fig. 2b), suggesting that, like previously shown for other SPX domains, PP-InsPs such as $InsP_7$ or $InsP_8$, may represent the *bona fide* Pi signalling molecule recognized/sensed by rice SPX2[22,26,30].

We next assessed the role of the domain-swapped SPX2 dimer in PHR2 binding. The intertwined dimer is mainly stabilized by hydrophobic and paired electrostatic interactions between the two anti-parallel helices α3. The hydrophobic network encompasses W18, F84, F87 and F88 from one protomer, and L129, L130, Y133 and N137 from another protomer (Fig. 2d). Substitutions of key residues in the network disrupted the PHR2 – SPX2 complex in vitro, whereas a substitution outside the hydrophobic network, R19A, had little impact on PHR2 – SPX2 complex association (Figs. 2d, e). The paired electrostatic interactions involve R105, E112 and E119 from one protomer, and E119, E112 and R105 from another protomer (Fig. 2d). Charge reversal mutation of these residues (R105E, E112R, and E119R) in the SPX2 dimer, that breaks paired electrostatic interactions, also abolished the binding of PHR2 (Figs. 2d, e). These residues contributing to SPX2 dimerization are well conserved in the stand-alone SPX proteins (Supplementary Fig. 3), supporting their importance in the dimerization of SPX proteins for the binding of PHR transcription factors.

We next assessed the interaction interface between SPX2 and PHR2 in vitro pull-down assays. Two copies of PHR2 are wrapped around the domain-swapped SPX2 dimer (Fig. 3a). The MYB domain and CC domain of PHR2 mainly interacts with the helix α3 of protomer A, and helices α3 and α5 of the protomer B in the SPX2 dimer, respectively. Residues R250, E257, H294, K297, Y298 and R302 in the MYB domain, and E92, E93, K100, E101 and E104 in the helix α3 of SPX2 protomer A, mediate the $PHR2^{MYB}$ – SPX2 association. The interaction between the CC domain and SPX2 is stabilized by residues Q345, K346, H349, E353 and R356 in the CC domain and H124, E131, T172, Y176, E183 and D187 in the helices α3 and α5 of SPX2 protomer B (Fig. 3a). Consistent with this, mutations of these key interacting residues in the $PHR2^{MYB}$ – SPX2 interface or in the $PHR2^{CC}$ – SPX2 interface disrupted the association of SPX2 and PHR2 (Figs. 3b, c). We also validated these interactions by in vitro pull-down analyses using rice SPX4, a homolog of rice SPX2 (Supplementary Fig. 8).

We next tested if SPX – PHR complex interface mutations can modulate the function of the related PHR1 transcription factor in *Arabidopsis*. We expressed wildtype and point mutant versions of PHR1 from its native promoter in the previously characterized *phr1 phl1* loss-of-function mutant[14] and scored growth phenotypes of the T1 transformants (Supplementary Figs. 9a, b). We found that plants carrying mutations in the PHR^{CC} – SPX interface ($AtPHR1^{L331A}$; L352 in OsPHR2 and $AtPHR1^{L339A}$; L360 is

OsPHR2) exhibited a growth phenotype similar to the parental *phr1 phl1* line, suggesting that these mutations may disrupt the SPX – PHR complex and possibly AtPHR1 oligomerisation[25]. We thus mutated additional polar residues in the PHR^{CC} – SPX complex interface that are located outside the AtPHR1 oligomerisation interface in the previously reported AtPHR1 CC structure[25]. We found that the mutations of $AtPHR1^{Q324A}$ (Q345 in OsPHR2), $AtPHR1^{E332A}$ (E353 in OsPHR2) and $AtPHR1^{E342A}$ (E363 in OsPHR2) resulted in severe dominant-negative growth phenotypes, that were reminiscent of the previously characterized $AtPHR1^{KHR}$ mutant, which cannot bind SPX proteins and thus represents a constitutively active transcription factor[25] (Supplementary Figs. 9a, b). Taken together, these and previously characterized[25] PHR^{CC} – SPX interface mutations can release PHR transcription factors from the regulation by SPX domains and PP-InsPs, leading to autoactivation.

To gain insights into how rice SPX2 reduces the DNA binding ability of PHR2, we determined the structure of the PHR2 MYB domain in complex with P1BS motif at 2.7 Å resolution (Fig. 4a, and Supplementary Table 1). It turns out that two MYB molecules are coordinated into the major groove of the imperfect palindromic DNA mainly through helices α3. The P1BS recognition by MYB is mediated by the interaction between the residues K292, S293 and Q296 in MYB and the nucleotides G7, A9, A11, G4', A6' and A8' in P1BS (Fig. 4b). Electrophoretic mobility shift assay (EMSA) results revealed that alanine substitution of theses residues attenuated the DNA binding ability of PHR2, and the charge reversal mutation of K292 abolished this interaction (Supplementary Fig. 10a). The structure of rice MYB/P1BS complex is consistent with classical binding models[31], and is similar to the reported structure of the AtPHR1 MYB in complex with P1BS (Supplementary Fig. 10b)[24].

We next compared the $PHR2^{MYB}$ – SPX2 and $PHR2^{MYB}$ – DNA complex interfaces and isolated amino-acids that contribute to the formation of the $PHR2^{MYB}$ – SPX2 complex, while being located outside the P1BS recognition site of the PHR2 MYB domain (Supplementary Figs. 9a, c). *In vivo*, mutation of $AtPHR1^{R229}$ (R250 in OsPHR2) or $AtPHR1^{H273/K276}$ (H294 and K297 in OsPHR2) to alanine again resulted in strong dominant growth phenotypes in the *phr1 phl1* mutant background (Supplementary Figs. 9a, b), indicating that also the $PHR2^{MYB}$ domain may contribute to PHR – SPX complex formation in *vivo*.

Structures of SPX2/$InsP_6$/PHR2 complex and MYB/DNA complex provide a framework for understanding how SPX2 senses the PP-InsP signal and transduces this signal into transcription inhibition. Superposing the two complex structures using the MYB domains as a reference, the position of SPX2 molecules heavily overlapped with the DNA position in the MYB/DNA complex, indicating that the binding of $InsP_6$-bound SPX2 to PHR2 would produce severe steric clashes and thus preventing DNA binding (Fig. 4c). It has been previously established that the CC domain of PHRs enables oligomerisation of the transcription factor critical for DNA binding[17,25]. In line with this, EMSA results showed that the DNA binding ability of $PHR2^{MYB\text{-}CC}$ is stronger than PHR^{MYB} (Supplementary Fig. 10c). Mutation of K325, H328 and R335 at the surface of AtPHR1 CC domain disrupted its interaction with SPX receptors, and led to constitutive Pi starvation responses[25], whereas the mutation of R318 or R340 produced no effect[25].

Mechanistically, our structure shows that these residues K346, H349 and R356 in OsPHR2 (corresponding to K325, H328 and R335 in AtPHR1) interact with OsSPX2, whereas R339 and R361 (corresponding to R318 and R340 in AtPHR1) do not contribute to the formation of the signalling complex (Fig. 4d, and Figs. 3a, c).

We have previously reported that the residues L319, I333 and L337 in AtPHR1 stabilize the CC oligomer required for DNA/promoter binding[25]. Our complex structure now uncovers the mechanism by which rice SPX2 disassembles PHR2 CC oligomers and impairs DNA binding. Specifically, SPX2 blocks the assembly of $PHR2^{CC}$ oligomers by exposing hydrophobic residues normally contributing to the stabilization of the coiled-coil structure (including L340, I354 and L358 that correspond to the previously characterized L319, I333 and L337 in AtPHR1)[25] (Fig. 4d). Collectively, the domain-swapped SPX2 dimer senses the $InsP_6$ / PP-InsP nutrient messenger to repress the PHR2 transcriptional activity by two distinct mechanisms: 1) The association of the $InsP_6$-bound SPX2 establishes severe steric clashes with the MYB domain, preventing DNA binding 2) Disruption of the CC domain oligomerisation motif in PHR2 attenuates its transcriptional activity (Figs. 4c, d).

Taken together, we propose a molecular model for the transcription inhibition of PHR2 by $InsP_6$ / PP-InsPs (Fig. 4e). Our structure clearly defines that in the case of PHR – SPX interactions, PP-InsPs do not act as "intermolecular glue" promoting the association of the signalling complex[32]. Instead, $InsP_6$ / PP-InsPs allosterically assemble a domain-swapped SPX2 dimer that targets two PHR2 monomers forming a 2:2:2 complex. Upon SPX2 dimer binding, the PHR2 CC domain can not longer oligomerise and the PHR2 MYB domain is inaccessible to DNA binding, leading to PHR2 inactivation. This unique molecular mechanism of plant phosphate homeostasis provides a framework for the rational engineering of crops with improved Pi use efficiency.

Methods

Molecular cloning. The codon-optimized complementary DNA of full length rice *SPX2*, *SPX4* and *PHR2* were synthesized. *PHR2* was subcloned into a pET21b (Novagen) vector with a C-terminal 8×His tag. *SPX4* was constructed with a 6×His tag and a caspase drICE protease cleavage site at the N-terminus, and was subcloned into a pET15D vector. *SPX2* was cloned into a pBB75 vector without any tag. The site-specific mutations were introduced into *PHR2* or *SPX* genes by overlap PCR. All the constructs were verified by DNA sequencing.

Protein expression and purification. For the preparation of SPX2/PHR2 complex, the SPX2 and PHR2, or the particular boundary and mutants, were co-expressed in *E. coli* strain BL21(DE3) using Lysogeny broth (LB) medium. The cells were induced with 0.2 mM isopropyl-b-D-thiogalactoside (IPTG) and 1 mM $InsP_6$ at 16 °C for 12 h. Harvested cells were lysed by a high-pressure cell disrupter in a buffer containing 25 mM Tris–HCl pH 8.0,150 mM NaCl, 1 mM $InsP_6$. Target protein was collected from the supernatant and

purified over Ni^{2+} affinity resin and HiTrap Heparin column used in tandem. 1 mM $InsP_6$ was present during all the purification processes. The protein was further purified into homogeneity by gel-filtration chromatography (Superdex-200 Increase 10/300 GL, GE Healthcare) in a buffer containing 25 mM Tris–HCl pH 8.0, 150 mM NaCl, 5 mM DTT and 1mM $InsP_6$. Target fractions were collected for biochemistry experiments and supplied with 10 mM $InsP_6$ for crystallization.

PHR2 was expressed alone and purified similarly as the purification of SPX2/PHR2 complex, except there was no $InsP_6$ added.

SPX4 was expressed in *E. coli* strain BL21(DE3) using LB medium, and induced with 0.2 mM IPTG at 16 °C for 12 h. Harvested cells were lysed, and the target protein was purified over Ni^{2+} affinity resin. After removal of the His tag by drICE protease, target protein was further purified over Source 15Q and Superdex-200 Increase 10/300 columns used in tandem. The protein was finally prepared in a buffer containing 25 mM Tris-HCl pH 8.0, 150 mM NaCl and 1 mM $InsP_6$.

MYB domain of PHR2 (residues 180-313) was expressed in *E. coli* strain BL21(DE3) using LB medium, and induced with 0.2 mM IPTG at 16 °C for 16 h. Harvested cells were lysed, and the target protein was purified over Ni^{2+} affinity resin, Source 15Q, and Superdex-200 Increase 10/300 columns used in tandem. The protein was final prepared in a buffer containing 25 mM Tris-HCl pH 8.0, 150 mM NaCl, 5 mM $MgCl_2$, and 5 mM DTT. For crystallization trials, the PHR2 MYB was incubated with the P1BS (5'-gCTTGAGGATATCCGA-3' and 5'-cTCGGATATCCTCAAG-3') in a molar ratio of 1:1.5 at 4 °C for about 30 min.

Crystallization. Crystallization experiments were performed through hanging-drop vapour-diffusion methods by mixing the protein with an equal volume of reservoir solution at 18 °C. The $mH2A1.1^{181-366}$ tagged $SPX2^{1-202/\Delta 47-59}/InsP_6/PHR2^{225-362}$ complex gave rise to best crystals under the condition of 8.4% PEG5000 MME, 6.5% Tacsimate pH 7.0, 0.15 M $(NH4)_2SO_4$, 0.1 M HEPES pH 6.8, 2.67% Pentaerythritol ethoxylate (3/4 EO/OH). Crystals were equilibrated in a cryoprotectant buffer containing 8%-12% PEG5000 MME, 5% Tacsimate pH 7.0, 0.1 M $(NH4)_2SO_4$, 0.1 M HEPES pH 7.0, 0.1 M KCl, 1.5 M L-Proline. By stepwise dehydration in the air, the crystal quality was improved. Finally, a best crystal from thousands of dehydrated crystals diffracted to 3.1 Å at Shanghai Synchrotron Radiation Facility beamline BL17U.

To crystalize the MYB domain of rice PHR2 (residues 180-313) in complex with DNA, the purified MYB was concentrated to about 200 μM and incubated with double-strand DNA (5'-gCTTGAGGATATCCGA-3' and 5'-cTCGGATATCCTCAAG-3'). The crystal of MYB/DNA complex was grown in 13% (w/v) PEG 3350, 0.1 M sodium malonate pH 6.0. The crystals were flash frozen in liquid nitrogen using 25% glycerol as the cryoprotective buffer and diffracted to 2.7 Å.

Data collection and structure determination. X-ray diffraction datasets of mH2A1.1$^{181-366}$-tagged SPX2$^{1-202/\Delta47-59}$/InsP$_6$/PHR2$^{225-362}$ complex and MYB/DNA complex were collected at the Shanghai Synchrotron Radiation Facility (SSRF) on beamline BL17U or BL19U[33,34]. The data were integrated and processed with the HKL2000 program suite or in XDS package[35]. Further data processing was carried out using CCP4 suit[36]. Crystal structures of the mH2A1.1$^{181-366}$-tagged SPX2$^{1-202/\Delta47-59}$/InsP$_6$/PHR2$^{225-362}$ complex and MYB/DNA complex were determined at resolutions of 3.1 Å, 2.7 Å, respectively. The structure of MYB/DNA was solved by molecular replacement using MYB domain of AtPHR1 (PDB ID 6J4R) as a search template. Using the resolved MYB domain and the human histone mH2A1.1 (PDB ID 1ZR3) as search the models, we determined the structure of mH2A1.1$^{181-366}$-tagged SPX2$^{1-202/\Delta47-59}$/InsP$_6$/PHR2$^{225-362}$ complex through molecular replacement by the program PHASER[37]. All the structures were iteratively built with COOT[38] and refined using PHENIX program[39]. Data collection and structure refinement statistics were summarized in Supplementary Table 1. All figures were generated using the PyMOL program (http://www.pymol.org/).

Analytical ultracentrifugation (AUC). The AUC experiment was performed in a Beckman Coulter XL-I analytical ultracentrifuge using two-channel centerpieces. The SPX2$^{1-280}$/PHR2$^{225-362}$ complex was prepared in a solution of 25 mM Tris-HCl pH8.0, 1mM InsP$_6$, and 150 mM NaCl. Data was collected via absorbance detection at 18 °C for protein at a concentration of 0.7 mg ml^{-1} and rotor speed of 45,000 r.p.m. The SV-AUC data were globally analyzed using the SEDFIT program and fitted to a continuous c(s) distribution model to determine the molecular weight.

Small angle X-ray scattering (SAXS). SAXS data were collected at the BL19U2 beamline of the Shanghai Synchrotron Radiation Facility (SSRF) at room temperature. 30 μM SPX2$^{1-202}$/PHR2$^{225-362}$ complex was prepared in the buffer of 25 mM Tris–HCl pH 8.0, 150 mM NaCl, 5 mM DTT and 1mM InsP$_6$ for SAXS measurement. For each measurement, 20 consecutive frames of 1-sec exposure were recorded and averaged, providing no difference between the first and the last frames. The background scattering was recorded for the matching buffer and was subtracted from the protein scattering data. The SAXS experiment was performed at room temperature. The data was visualized and analyzed using the software package ATSAS[40]. For the calculation of the theoretical SAXS profile of SPX2$^{1-202}$/InsP$_6$/PHR2$^{225-362}$ complex, the invisible residues of the crystal structure were build using PyMOL and are refined by Xplor-NIH[41]. The theoretical SAXS profile was calculated using CRYSOL of software package ATSAS[40].

Thiol-directed chemical crosslinking. The complex of SPX2$^{1-280}$/PHR2$^{225-362}$, SPX2$^{1-280}$_K106C/PHR2$^{225-362}$ and SPX2$^{1-280}$_K106C/C182S /PHR2$^{225-362}$ was prepared in a buffer containing 25 mM Tris–HCl pH 8.0, 150 mM NaCl and 1mM InsP$_6$, respectively. About 30 mM complex protein was incubated with 200 mM M2M (1,2-ethanediyl bismethanethiosulfonate) at room temperature for 30 min. The reaction mixture was analyzed by SDS-PAGE and Coomassie Blue staining in the condition of 100 mM DTT, or not.

Co-expression coupled Ni-NTA pull-down. We have tried various expression systems, such as *E. Coli*., *insects*, or *mammalian* cells, to express the SPX2 alone, but no soluble SPX2 protein was obtained. Therefore, we applied a co-expression coupled Ni-NTA pull-down strategy to assess ligand binding and protein interactions (Supplementary Fig. 2). In this system, no tag SPX2 was co-expressed with 8×His-tagged PHR2, and then supernatant of the lysed cells were loaded on Ni-NTA beads. After washing unbound proteins, the His-tagged PHR2 and interacting SPX2 were co-eluted by imidazole.

Since the SPX2/PHR2 association is $InsP_6$ dependent (Supplementary Fig. 2)[22,26], the loss of $InsP_6$ binding ability will make SPX2 no longer interact with PHR2. Thus, the Ni-NTA pull-down assay of SPX2/PHR2 association by co-expressing His-tagged PHR2 with SPX2, or SPX2 mutants, in the presence of $InsP_6$, can be used to assess the recognition of $InsP_6$ by SPX2 (Fig. 2c). Similarly, we used this strategy assessed the role of SPX2 domain-swapped dimer in PHR2 recognition (Fig, 2e), and revealed keys residues for the interaction between SPX2 and PHR2 (Figs. 3b, c).

In *vitro* pull-down assay of SPX4 and PHR2. SPX4 and PHR2 was prepared in a buffer containing 25 mM Tris-HCl pH 8.0, 150 mM NaCl and 1 mM $InsP_6$, respectively. About 20 mM SPX4 was incubated with 20 mM PHR2 on ice for 30 minutes. Then the mixture was loaded onto Ni-NTA beads and incubated for 30 minutes. After extensively washing with a buffer containing 25 mM Tris-HCl pH 8.0, 150 mM NaCl, 15 mM imidazole and 1 mM $InsP_6$, the bound protein was eluted by a buffer containing 25 mM Tris-HCl pH 8.0, 150 mM NaCl, 250 mM imidazole and 1 mM $InsP_6$. The input protein and eluted fractions were analyzed by SDS-PAGE and Coomassie Blue staining.

Generation of constructs and transgenic lines. Binary constructs were generated using the Golden Gate system[42]. For Level I constructs, the full-length *AtPHR1* coding sequence and the *AtPHR1* promoter (pPHR1, 265bp) were cloned into pUC-BpiI via BpiI cut-ligation. Mutations targeting the *AtPHR1* coding sequence were introduced by site-directed mutagenesis on the resulting Level I plasmid, as previously described[43] (primers are listed in Supplementary Table 2). Level I constructs were assembled in Level II constructs via BsaI cut-ligation (constructs are listed in Supplementary Table 2). All constructs were transformed into *Agrobacterium tumefaciens* strain pGV3101. Plants were transformed using the floral dip method[44]. Transformants were identified by FastRed fluorescence with a Zeiss Axio Zoom.V16 stereomicroscope (mRFP filter) and a HXP200C illuminator.

Plant material and growth conditions. All experiments were done in *Arabidopsis thaliana* Colombia (Col-0) ecotype. Arabidopsis *phr1 phl1 s*eeds[14] were kindly provided by Dr. Yves Poirier (University of Lausanne, Switzerland). Plants were grown at 21°C, 60% humidity and in a 16/8 hour light/dark cycle.

Electrophoretic mobility shift assay (EMSA). FAM-labeled primers were used to generate the DNA fragment (F:5'-AAGCTTGAATATGCAATGGAATATGCTTAG-3', R:5'-CTAAGCATATTCCATTGCATATTCAAGCTT-3'). The DNA fragment was annealed by heating to 95 °C for 5 min and gradually cooled to 25 °C. The FAM-labelled DNA (10 nM) was incubated with 0.3375, 0.45, 0.6, and 0.8 mM PHR2 proteins at 4 °C for 30 min, in a buffer of 25 mM Tris–HCl pH 8.0, 150 mM NaCl, 5 mM

DTT, 10% glycerol, and 200 ng ml^{-1} Heparin. The reactions were resolved on 8% native acrylamide gels (37.5:1 acrylamide:bis-acrylamide) in 0.5× Tris–Boric acid buffer at 150 V for about 3 h. Images of the gels were obtained using FLA5100(Typhoon, Fuji, Japan).

Declarations

Data Availability

Atomic coordinates of SPX2/$InsP_6$/PHR2 and $PHR2^{MYB}$/DNA complex have been deposited in the Protein Data Bank (PDB) under accession number 7D3Y and 7D3T, respectively.

Acknowledgements

We thank staffs at the BL17U, BL19U and BL19U2 beamline of the NCPSS at Shanghai Synchrotron Radiation Facility for assistance with data collection, and research associate Dr. De-lin Zhang at the Center for Protein Research, Huazhong Agricultural University, for facilities support. We thank Prof. Lizhong Xiong for helpful discussions. The work has been supported by the National Key R&D Program of China (2018YFA0507700 to Z.L.), and by the National Natural Science Foundation of China (32071226 to Z.L.), by the Fundamental Research Funds for the Central Universities (Program No. 2662019PY004 to Z.L.), and by the European Union's Horizon 2020 research program under ERC consolidator grant agreement 818696 (INSPIRE) to M.H.. Zeyuan Guan also acknowledges the support of National Postdoctoral Program for Innovative Talents (BX2021108).

Author contributions

Z.L. and Z.Y.G. conceived the project and designed the experiments, Z.Y.G., Q.X.Z. and Z.F.Z. performed crystallization and resolved the structures, J.S., L.B. and M.H. designed and performed the genetic experiments, J.Q.Z., J.C., P.C., Q.W., K.P., D.L.Z., T.T.Z., J.J.Y. and P.Y. performed biochemistry experiments and analyzed data. Z.L. and M.H. wrote the manuscript with support from all authors.

Author information

Correspondence and requests for materials should be addressed to Z.L. (liuzhu@mail.hzau.edu.cn). Z.Y.G., Q.X.Z. and Z.F.Z. contributed equally to this research.

Competing interests

The authors declare no competing interests.

References

1 Oldroyd, G. E. D. & Leyser, O. A plant's diet, surviving in a variable nutrient environment. *Science* **368** (2020).

2 Gong, Z. Z., Xiong, L. M., Shi, H. Z., Yang, S. H., Herrera-Estrella, L. R., Xu, G. H., Chao, D. Y., Li, J. R., Wang, P. Y., Qin, F., Li, J. J., Ding, Y. L., Shi, Y. T., Wang, Y., Yang, Y. Q., Guo, Y. & Zhu, J. K. Plant abiotic stress response and nutrient use efficiency. *Science China-Life Sciences* **63**, 635-674 (2020).

3 Raghothama, K. G. Phosphate Acquisition. *Annu Rev Plant Physiol Plant Mol Biol* **50**, 665-693 (1999).

4 Vance, C. P., Uhde-Stone, C. & Allan, D. L. Phosphorus acquisition and use: critical adaptations by plants for securing a nonrenewable resource. *New Phytologist* **157**, 423-447 (2003).

5 Rouached, H., Arpat, A. B. & Poirier, Y. Regulation of phosphate starvation responses in plants: signaling players and cross-talks. *Mol Plant* **3**, 288-299 (2010).

6 Chiou, T. J. & Lin, S. I. Signaling network in sensing phosphate availability in plants. *Annu Rev Plant Biol* **62**, 185-206 (2011).

7 Wu, P., Shou, H., Xu, G. & Lian, X. Improvement of phosphorus efficiency in rice on the basis of understanding phosphate signaling and homeostasis. *Curr Opin Plant Biol* **16**, 205-212 (2013).

8 Lopez-Arredondo, D. L., Leyva-Gonzalez, M. A., Gonzalez-Morales, S. I., Lopez-Bucio, J. & Herrera-Estrella, L. Phosphate nutrition: improving low-phosphate tolerance in crops. *Annu Rev Plant Biol* **65**, 95-123 (2014).

9 Ham, B. K., Chen, J. Y., Yan, Y. & Lucas, W. J. Insights into plant phosphate sensing and signaling. *Current Opinion in Biotechnology* **49**, 1-9 (2018).

10 Jung, J. Y., Ried, M. K., Hothorn, M. & Poirier, Y. Control of plant phosphate homeostasis by inositol pyrophosphates and the SPX domain. *Curr Opin Biotechnol* **49**, 156-162 (2018).

11 Misson, J., Raghothama, K. G., Jain, A., Jouhet, J., Block, M. A., Bligny, R., Ortet, P., Creff, A., Somerville, S., Rolland, N., Doumas, P., Nacry, P., Herrerra-Estrella, L., Nussaume, L. & Thibaud, M. C. A genome-wide transcriptional analysis using Arabidopsis thaliana Affymetrix gene chips determined plant responses to phosphate deprivation. *Proc Natl Acad Sci U S A* **102**, 11934-11939 (2005).

12 Morcuende, R., Bari, R., Gibon, Y., Zheng, W., Pant, B. D., Blasing, O., Usadel, B., Czechowski, T., Udvardi, M. K., Stitt, M. & Scheible, W. R. Genome-wide reprogramming of metabolism and regulatory networks of Arabidopsis in response to phosphorus. *Plant Cell Environ* **30**, 85-112 (2007).

13 Lee, Y. S., Mulugu, S., York, J. D. & O'Shea, E. K. Regulation of a cyclin-CDK-CDK inhibitor complex by inositol pyrophosphates. *Science* **316**, 109-112 (2007).

14 Bustos, R., Castrillo, G., Linhares, F., Puga, M. I., Rubio, V., Perez-Perez, J., Solano, R., Leyva, A. & Paz-Ares, J. A central regulatory system largely controls transcriptional activation and repression responses to phosphate starvation in Arabidopsis. *PLoS Genet* **6**, e1001102 (2010).

15 Wykoff, D. D., Grossman, A. R., Weeks, D. P., Usuda, H. & Shimogawara, K. Psr1, a nuclear localized protein that regulates phosphorus metabolism in Chlamydomonas. *Proc Natl Acad Sci U S A* **96**, 15336-15341 (1999).

16 Rubio, V., Linhares, F., Solano, R., Martin, A. C., Iglesias, J., Leyva, A. & Paz-Ares, J. A conserved MYB transcription factor involved in phosphate starvation signaling both in vascular plants and in unicellular algae. *Genes & Development* **15**, 2122-2133 (2001).

17 Zhou, J., Jiao, F., Wu, Z., Li, Y., Wang, X., He, X., Zhong, W. & Wu, P. OsPHR2 is involved in phosphate-starvation signaling and excessive phosphate accumulation in shoots of plants. *Plant Physiol* **146**, 1673-1686 (2008).

18 Guo, M., Ruan, W., Li, C., Huang, F., Zeng, M., Liu, Y., Yu, Y., Ding, X., Wu, Y., Wu, Z., Mao, C., Yi, K., Wu, P. & Mo, X. Integrative Comparison of the Role of the PHOSPHATE RESPONSE1 Subfamily in Phosphate Signaling and Homeostasis in Rice. *Plant Physiol* **168**, 1762-1776 (2015).

19 Wang, Z., Ruan, W., Shi, J., Zhang, L., Xiang, D., Yang, C., Li, C., Wu, Z., Liu, Y., Yu, Y., Shou, H., Mo, X., Mao, C. & Wu, P. Rice SPX1 and SPX2 inhibit phosphate starvation responses through interacting with PHR2 in a phosphate-dependent manner. *Proc Natl Acad Sci U S A* **111**, 14953-14958 (2014).

20 Lv, Q. D., Zhong, Y. J., Wang, Y. G., Zhang, L., Shi, J., Wu, Z. C., Liu, Y., Mao, C. Z., Yi, K. K. & Wu, P. SPX4 Negatively Regulates Phosphate Signaling and Homeostasis through Its Interaction with PHR2 in Rice. *Plant Cell* **26**, 1586-1597 (2014).

21 Puga, M. I., Mateos, I., Charukesi, R., Wang, Z., Franco-Zorrilla, J. M., de Lorenzo, L., Irigoyen, M. L., Masiero, S., Bustos, R., Rodriguez, J., Leyva, A., Rubio, V., Sommer, H. & Paz-Ares, J. SPX1 is a phosphate-dependent inhibitor of Phosphate Starvation Response 1 in Arabidopsis. *Proc Natl Acad Sci U S A* **111**, 14947-14952 (2014).

22 Wild, R., Gerasimaite, R., Jung, J. Y., Truffault, V., Pavlovic, I., Schmidt, A., Saiardi, A., Jessen, H. J., Poirier, Y., Hothorn, M. & Mayer, A. Control of eukaryotic phosphate homeostasis by inositol polyphosphate sensor domains. *Science* **352**, 986-990 (2016).

23 Zhong, Y., Wang, Y., Guo, J., Zhu, X., Shi, J., He, Q., Liu, Y., Wu, Y., Zhang, L., Lv, Q. & Mao, C. Rice SPX6 negatively regulates the phosphate starvation response through suppression of the transcription factor PHR2. *New Phytol* **219**, 135-148 (2018).

24 Jiang, M., Sun, L., Isupov, M. N., Littlechild, J. A., Wu, X., Wang, Q., Wang, Q., Yang, W. & Wu, Y. Structural basis for the Target DNA recognition and binding by the MYB domain of phosphate starvation response 1. *FEBS J* **286**, 2809-2821 (2019).

25 Ried, M. K., Wild, R., Zhu, J., Pipercevic, J., Sturm, K., Broger, L., Harmel, R. K., Abriata, L. A., Hothorn, L. A., Fiedler, D., Hiller, S. & Hothorn, M. Inositol pyrophosphates promote the interaction of SPX

domains with the coiled-coil motif of PHR transcription factors to regulate plant phosphate homeostasis. *Nat Commun* **12**, 384 (2021).

26 Dong, J., Ma, G., Sui, L., Wei, M., Satheesh, V., Zhang, R., Ge, S., Li, J., Zhang, T. E., Wittwer, C., Jessen, H. J., Zhang, H., An, G. Y., Chao, D. Y., Liu, D. & Lei, M. Inositol Pyrophosphate InsP8 Acts as an Intracellular Phosphate Signal in Arabidopsis. *Mol Plant* **12**, 1463-1473 (2019).

27 Wild, R. & Hothorn, M. The macro domain as fusion tag for carrier-driven crystallization. *Protein Sci* **26**, 365-374 (2017).

28 Holm, L. & Sander, C. Protein structure comparison by alignment of distance matrices. *J Mol Biol* **233**, 123-138 (1993).

29 Holm, L., Kaariainen, S., Rosenstrom, P. & Schenkel, A. Searching protein structure databases with DaliLite v.3. *Bioinformatics* **24**, 2780-2781 (2008).

30 Zhu, J., Lau, K., Puschmann, R., Harmel, R. K., Zhang, Y., Pries, V., Gaugler, P., Broger, L., Dutta, A. K., Jessen, H. J., Schaaf, G., Fernie, A. R., Hothorn, L. A., Fiedler, D. & Hothorn, M. Two bifunctional inositol pyrophosphate kinases/phosphatases control plant phosphate homeostasis. *Elife* **8** (2019).

31 Dubos, C., Stracke, R., Grotewold, E., Weisshaar, B., Martin, C. & Lepiniec, L. MYB transcription factors in Arabidopsis. *Trends Plant Sci* **15**, 573-581 (2010).

32 Desmarini, D., Lev, S., Furkert, D., Crossett, B., Saiardi, A., Kaufman-Francis, K., Li, C., Sorrell, T. C., Wilkinson-White, L., Matthews, J., Fiedler, D. & Djordjevic, J. T. IP7-SPX Domain Interaction Controls Fungal Virulence by Stabilizing Phosphate Signaling Machinery. *mBio* **11** (2020).

33 Wang, Q. S., Yu, F., Huang, S., Sun, B., Zhang, K. H., Liu, K., Wang, Z. J., Xu, C. Y., Wang, S. S., Yang, L. F., Pan, Q. Y., Li, L., Zhou, H., Cui, Y., Xu, Q., Earnest, T. & He, J. H. The macromolecular crystallography beamline of SSRF. *Nuclear Science and Techniques* **26**, 12-17 (2015).

34 Wang, Q. S., Zhang, K. H., Cui, Y., Wang, Z. J., Pan, Q. Y., Liu, K., Sun, B., Zhou, H., Li, M. J., Xu, Q., Xu, C. Y., Yu, F. & He, J. H. Upgrade of macromolecular crystallography beamline BL17U1 at SSRF. *Nuclear Science and Techniques* **29** (2018).

35 Otwinowski, Z. & Minor, W. Processing of X-ray diffraction data collected in oscillation mode. *Methods Enzymol* **276**, 307-326 (1997).

36 Winn, M. D., Ballard, C. C., Cowtan, K. D., Dodson, E. J., Emsley, P., Evans, P. R., Keegan, R. M., Krissinel, E. B., Leslie, A. G., McCoy, A., McNicholas, S. J., Murshudov, G. N., Pannu, N. S., Potterton, E. A., Powell, H. R., Read, R. J., Vagin, A. & Wilson, K. S. Overview of the CCP4 suite and current developments. *Acta Crystallogr D Biol Crystallogr* **67**, 235-242 (2011).

37 McCoy, A. J., Grosse-Kunstleve, R. W., Adams, P. D., Winn, M. D., Storoni, L. C. & Read, R. J. Phaser crystallographic software. *J Appl Crystallogr* **40**, 658-674 (2007).

38 Emsley, P. & Cowtan, K. Coot: model-building tools for molecular graphics. *Acta Crystallogr D Biol Crystallogr* **60**, 2126-2132 (2004).

39 Adams, P. D., Grosse-Kunstleve, R. W., Hung, L. W., Ioerger, T. R., McCoy, A. J., Moriarty, N. W., Read, R. J., Sacchettini, J. C., Sauter, N. K. & Terwilliger, T. C. PHENIX: building new software for automated crystallographic structure determination. *Acta Crystallogr D Biol Crystallogr* **58**, 1948-1954 (2002).

40 Franke, D., Petoukhov, M. V., Konarev, P. V., Panjkovich, A., Tuukkanen, A., Mertens, H. D. T., Kikhney, A. G., Hajizadeh, N. R., Franklin, J. M., Jeffries, C. M. & Svergun, D. I. ATSAS 2.8: a comprehensive data analysis suite for small-angle scattering from macromolecular solutions. *J Appl Crystallogr* **50**, 1212-1225 (2017).

41 Schwieters, C. D., Kuszewski, J. J. & Clore, G. M. Using Xplor-NIH for NMR molecular structure determination. *Progress in Nuclear Magnetic Resonance Spectroscopy* **48**, 47-62 (2006).

42 Lampropoulos, A., Sutikovic, Z., Wenzl, C., Maegele, I., Lohmann, J. U. & Forner, J. GreenGate—a novel, versatile, and efficient cloning system for plant transgenesis. *PLoS One* **8**, e83043 (2013).

43 Liu, H. & Naismith, J. H. An efficient one-step site-directed deletion, insertion, single and multiple-site plasmid mutagenesis protocol. *BMC Biotechnol* **8**, 91 (2008).

44 Clough, S. J. & Bent, A. F. Floral dip: a simplified method for Agrobacterium-mediated transformation of Arabidopsis thaliana. *Plant J* **16**, 735-743 (1998).

Figures

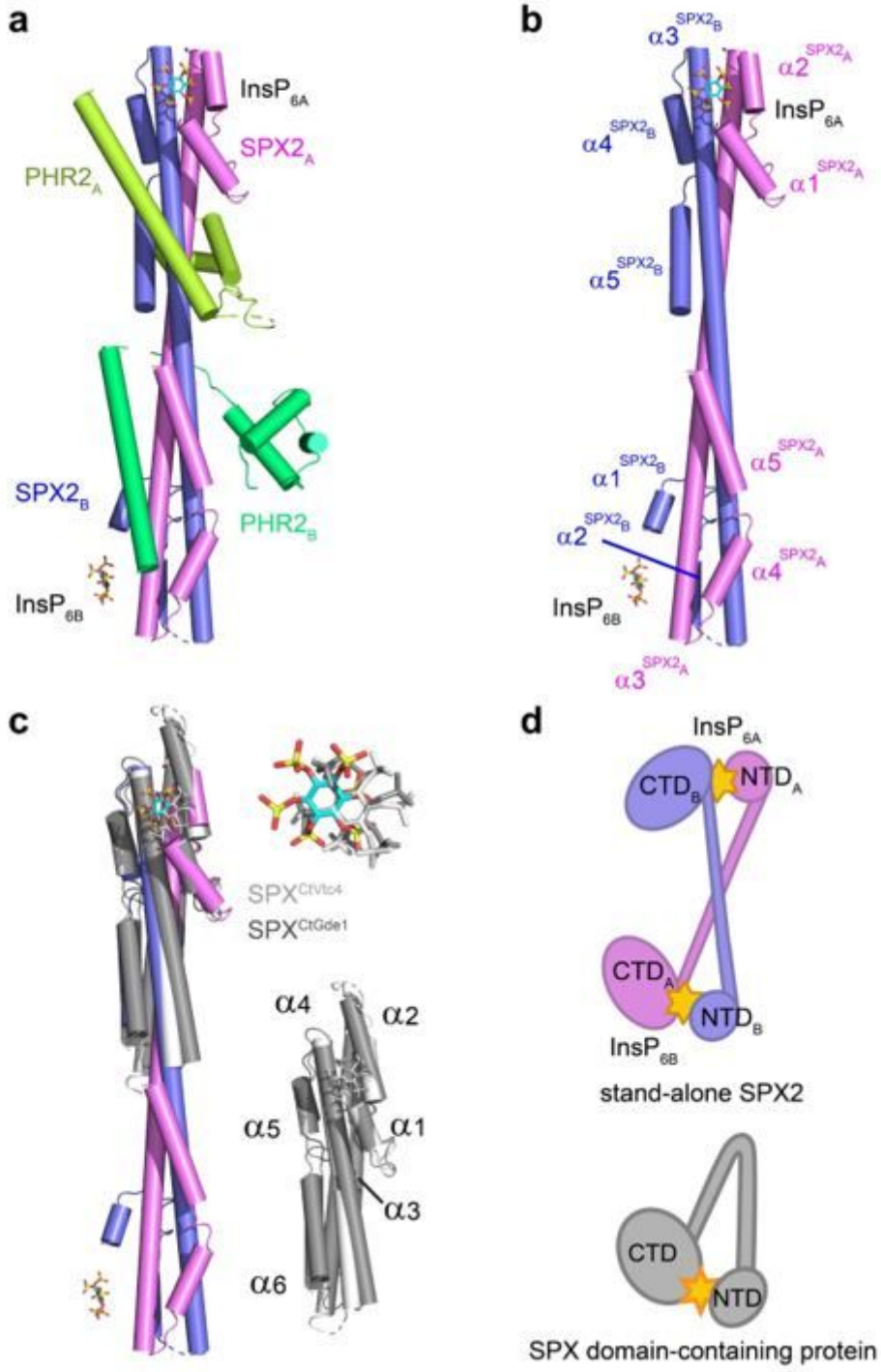

Figure 1

The structure of rice SPX2/InsP6/PHR2 complex and topology differences between the rice stand-alone SPX2 and SPX domain-containing proteins. a, Overall structure of the ternary complex. The protomers of the two SPX2 and the two PHR2 molecules are colored in magenta, blue, yellow, and green cartoon representation, respectively. InsP6 molecules are represented in sticks. b, Domain-swapped conformation of the SPX2 dimer. The α-helices of each protomer are numbered and highlighted in magenta and blue, respectively. c, Structural comparison between the stand-alone SPX2 dimer and other monomeric SPX

domain-containing proteins. SPX domain-containing proteins are colored in gray with numbered secondary structures. d, Topological diagrams of the stand-alone SPX2 other SPX domain-containing protein. InsP6 is represented in yellow star.

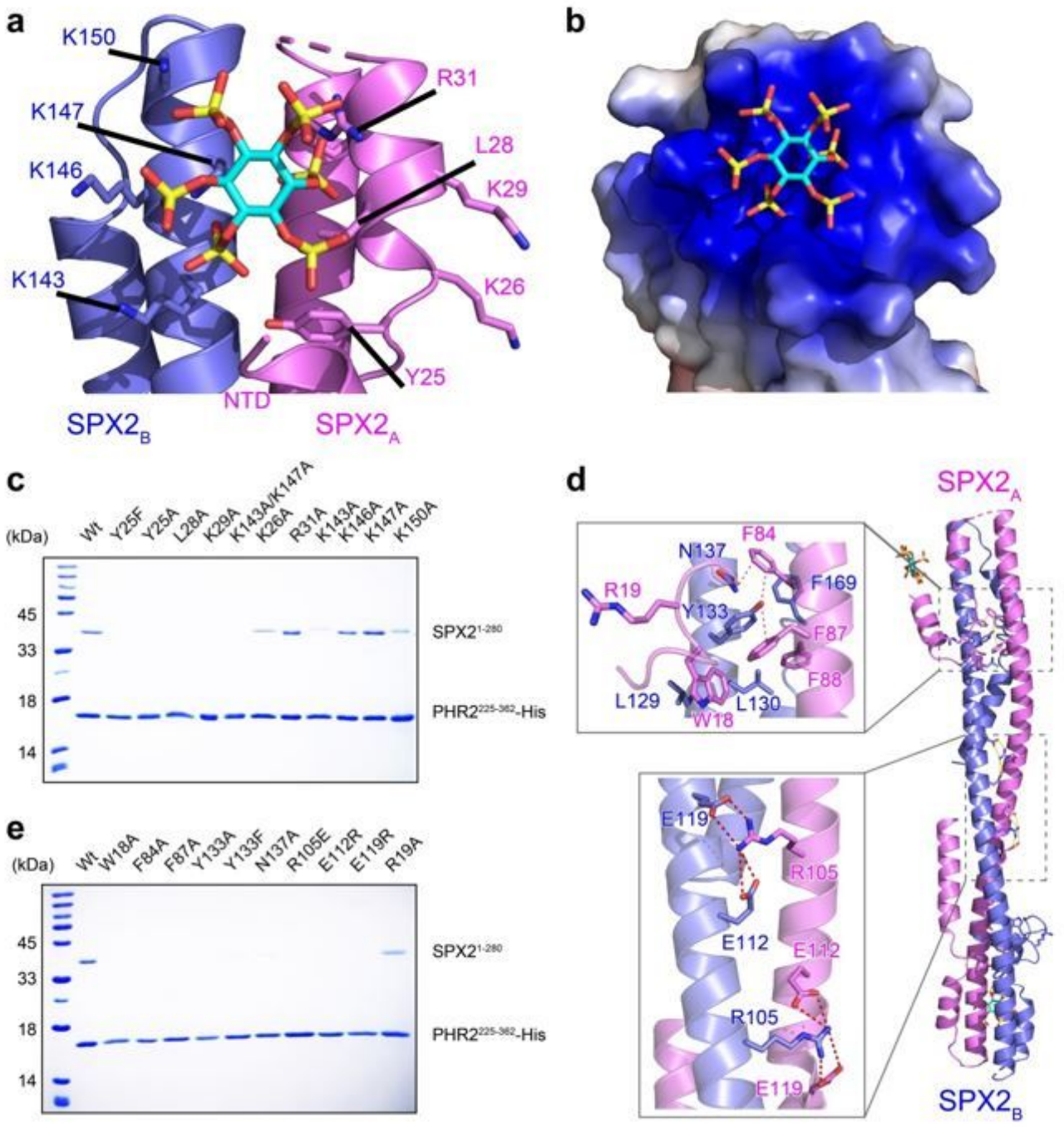

Figure 2

The recognition of InsP6 by the domain-swapped rice SPX2 dimer. a, Binding surface of InsP6 in the SPX2 dimer. b, The electrostatic surface of the InsP6 binding surface, colored in terms of electrostatic potential, and displayed in a scale from red (−5 kT/e) to blue (+5 kT/e). c, Co-expression coupled Ni-NTA pull-down assess the InsP6 binding for SPX2/PHR2 association. d, Interface of the SPX2 dimer. e, Co-

expression coupled Ni-NTA pull-down assess the SPX2 dimerization for SPX2/PHR2 association. For the pull-down assay, different mutated versions of the full length SPX21-280 and His-tagged PHR2225-362 were co-expressed in the presence of 1 mM InsP6.

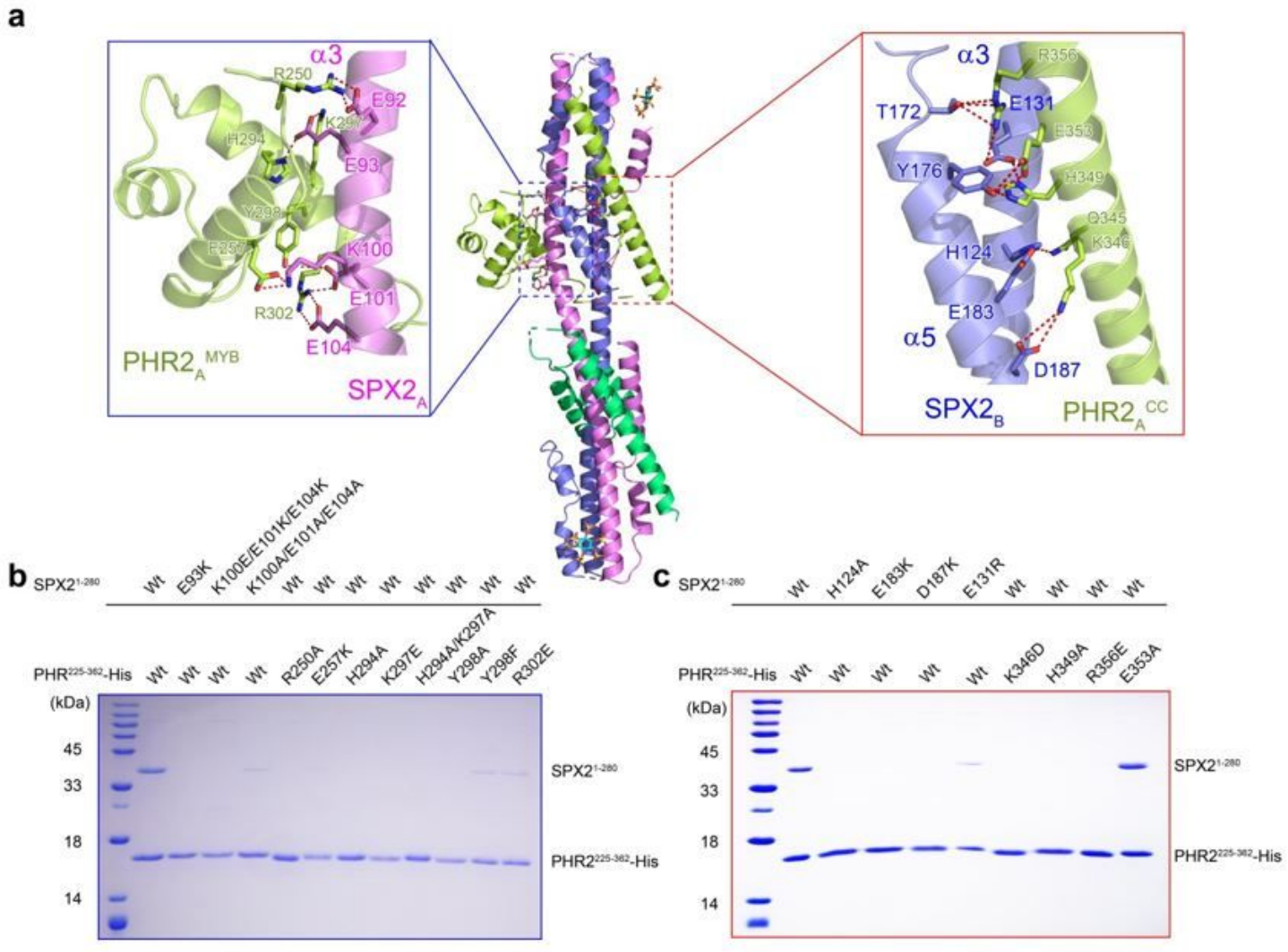

Figure 3

The recognition of rice PHR2 by the domain-swapped rice SPX2 dimer. a, The binding surface of the MYB domain and CC domain of PHR2A in the domain-swapped SPX2 dimer. The PHR2 protomer A binds to the SPX2 dimer in the same way as protomer B, and only the details of protomer A are depicted. b, Co-expression coupled Ni-NTA pull-down assess the interface between PHR2MYB and SPX2 dimer, and c, between PHR2CC and SPX2 dimer. For the pull-down assay, different mutated versions of the full length SPX21-280 and His-tagged PHR2225-362 were co-expressed in the presence of 1 mM InsP6.

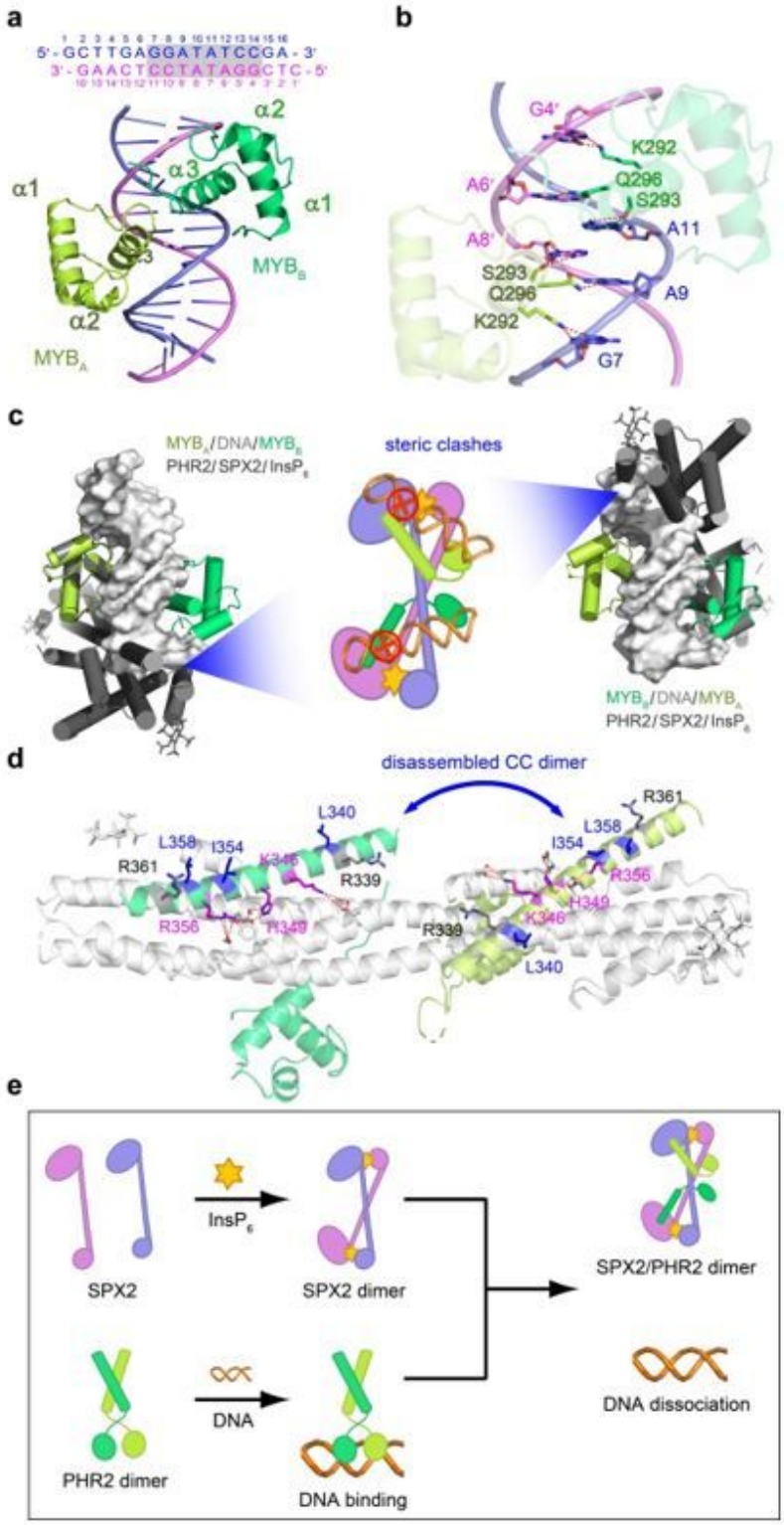

Figure 4

The mechanism of transcriptional repression of rice PHR2 by the InsP6-bound SPX2 binding. a, The structure of PHR2 MYB domain in complex with DNA. The P1BS motif is highlighted in gray shading. b, The interface between the MYB domain and P1BS motif. c, Structure superposition of MYB/DNA complex and SPX2/InsP6/PHR2 complex. They are aligned by superposing the MYB protomer A or B of MYB/DNA structure with the MYB domain of PHR2 protomer A or B in the SPX2/InsP6/PHR2 complex, respectively.

The two MYB molecules and DNA in the MYB/DNA complex are colored in yellow cartoon, green cartoon and gray surface representation, respectively. Steric clashes of PHR2 preventing DNA binding are illustrated in the middle model. d, Structural basis for InsP6-bound SPX2 disassembles the dimerization of PHR2 CC domain. Residues responsible for SPX2 binding and CC dimerization are highlighted in magenta and blue, respectively. No-interacting residues are colored in black. e, A model illustration for the transcription inhibition of PHR2 by InsP6 / PP-InsPs.

Supplementary Files

This is a list of supplementary files associated with this preprint. Click to download.

- SI20210624.docx
- s10.pdf
- s31.pdf
- s5.pdf
- s6.pdf
- s1.pdf
- s32.pdf
- s7.pdf
- s4.pdf
- s2.pdf
- s8.pdf
- s9.pdf